# Spin-valley coupling in a two-dimensional $VSi_2N_4$ monolayer

Qirui Cui,[1,2] Yingmei Zhu,[1] Jinghua Liang,[1] Ping Cui,[1,2] and Hongxin Yang[1,3,*]

[1]*Ningbo Institute of Materials Technology and Engineering, Chinese Academy of Sciences, Ningbo 315201, China*

[2]*Faculty of Science and Engineering, University of Nottingham Ningbo China, Ningbo 315100, China*

[3]*Center of Materials Science and Optoelectronics Engineering, University of Chinese Academy of Sciences, Beijing 100049, China*

(Received 18 November 2020; revised 28 January 2021; accepted 29 January 2021; published 15 February 2021)

Materials that integrate magnetism, miniaturization, and valley properties hold potential for spintronic and valleytronic nanodevices. Recently, ferromagnetism was reported to be able to exist in the $VSi_2N_4$ monolayer which is half-metallic and belongs to a new kind of two-dimensional material [Hong *et al.*, Science **369**, 670 (2020)]. Using first-principles calculations and model analysis, we find that $VSi_2N_4$ is a ferromagnetic semiconductor harboring valley-contrasting physics and a magnetic critical temperature over room temperature. By tuning magnetization orientation from in plane to out of plane, valley polarization can be generated, resulting in the anomalous valley Hall effect in $VSi_2N_4$. Furthermore, we obtain the formula for energy splitting of valleys and adopt a tight-binding model for $VSi_2N_4$, which elucidates the physical mechanism of spin-valley coupling. More interestingly, under 4% tensile strain, the intrinsic magnetic anisotropy of $VSi_2N_4$ becomes out of plane, and spontaneous valley polarization is achieved. Our results highlight that $VSi_2N_4$ is a good candidate for spintronic and valleytronic applications.

DOI: 10.1103/PhysRevB.103.085421

## I. INTRODUCTION

The valley, which indicates the maximum of valence bands or minimum of conduction bands, is a new degree of freedom of carriers besides the charge and spin. The valley degree of freedom can be used to encode, store, and transmit information, and due to large valley separation in reciprocal space, the valley index is robust against the scatterings of smooth deformations and phonons [1–5]. Therefore, materials with valley characteristics are very promising in the next-generation electronic devices with high storage density and low energy consumption [6]. Because of the inversion symmetry breaking of structures and strong spin-orbit coupling (SOC) from $d$ orbitals in transition-metal atoms, 2$H$-phase transition-metal dichalcogenides (2H TMDCs), such as $MoS_2$, $MoSe_2$, $WS_2$ and $WSe_2$, monolayers, have been demonstrated to be able to harbor valley physics, and some interesting phenomena including valley Hall effect [7,8], valley polarization [9,10], and the control of valley pseudospin [11–13] have been realized in these systems. The key for developing the practical valleytronic devices is inducing large valley polarization. Optical pumping with circularly polarized light can realize the valley polarization, but optical pumping is a dynamic process and requires complicated equipment, which is inconvenient for practical devices. Another approach is using magnetism, such as external magnetic field [14,15], magnetic doping [16,17], and magnetic proximity effects [18,19], to break valley degeneracy since the valleys are directly coupled with spin. However, the valley polarization induced by an external magnetic field is very small, about 0.1 meV/T: Magnetic dopants tend to form clusters limiting the quality of the systems and, for magnetic proximity effects, the substrate usually deforms electronic states of the host, and the interlayer interaction is easily influenced by surface defects. To overcome the above shortages, the materials are naturally required to process intrinsic long-range ferromagnetism or antiferromagnetism, miniaturization, and valley characters simultaneously.

Recently, $MoSi_2N_4$ and $WSi_2N_4$, which are a new type of two-dimensional (2D) layered material, were synthesized by the chemical vapor deposition (CVD) method; moreover, it has been theoretically reported that the $VSi_2N_4$ monolayer is a half-metallic ferromagnet and has the same crystal structure as $MoSi_2N_4$ and $WSi_2N_4$ [20]. In this paper, via first-principles calculations and model analysis, we unveil that $VSi_2N_4$ monolayer is a ferromagnetic (FM) semiconductor with valley properties. By tuning the magnetization orientation from in plane (IP) to out of plane (OOP), a large valley polarization of 63.11 meV can be achieved. Furthermore, we obtain a formula of energy splitting under SOC and adopt a tight-binding model, which elucidates the physical picture of spin-valley coupling in $VSi_2N_4$. The valley polarization and opposite Berry curvatures at $-K$ and $+K$ result in the anomalous valley Hall effect (AVHE) in $VSi_2N_4$ when magnetization orientation is OOP. More interestingly, under 4% tensile strain, the $VSi_2N_4$ monolayer can be tuned to a "ferrovalley" material [21] with a spontaneous valley polarization of 71.71 meV. These results demonstrate that $VSi_2N_4$ monolayer can be a good candidate for spintronic and valleytronic applications.

## II. CALCULATION METHOD

All first-principles calculations within density functional theory (DFT) are implemented in the Vienna *ab initio*

*hongxin.yang@nimte.ac.cn

 

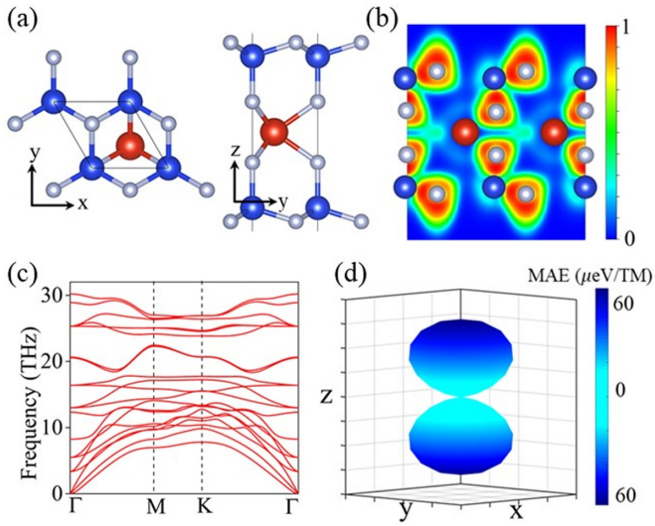


FIG. 1. (a) The top and side views of the crystal structure, (b) electron localization function, (c) phonon dispersions, and (d) magnetic anisotropy of $VSi_2N_4$ monolayer. In (a), (b), the red, gray, and blue balls represent V, N, and Si elements, respectively.

simulation package (VASP) [22–24]. The exchange-correlation interaction is treated by the generalized gradient approximation (GGA) based on the Perdew-Burke-Ernzerhof (PBE) function [25,26]. The cutoff energies for expanding plane wave basis are 520 eV, and the convergence criterion of electronic iteration is set to $10^{-7}$ eV. All structures are relaxed until Hellmann-Feynman force on each atom is less than 0.001 eV/Å. To describe strongly correlated $3d$ electrons of V [21,27], the GGA+$U$ method is applied ($U_{\text{eff}} = 3$ eV). Moreover, we compare band structures of $VSi_2N_4$ obtained from GGA+$U$ with that from the hybrid functional HSE06 [28], since the latter usually gives more accurate electronic states. The Brillouin zone is sampled using $17 \times 17 \times 1$ and $13 \times 13 \times 1$ Γ-center $k$-point grids for GGA+$U$ and HSE06, respectively. The phonon dispersions are calculated by the PHONOPY code [29] with a $4 \times 4 \times 1$ supercell. The maximally localized Wannier functions (MLWFs) calculated by the WANNIER90 package [30] are applied for obtaining the Berry curvature and anomalous Hall conductivity.

## III. RESULTS AND DISCUSSIONS

The crystal structure of a $VSi_2N_4$ monolayer is shown in Fig. 1(a). $VSi_2N_4$ consists of septuple layers of N-Si-N-V-N-Si-N, with atoms in each layer forming a two-dimensional (2D) hexagonal lattice. The central V atom is coordinated by six neighboring N atoms in a trigonal prismatic geometry, and then this $VN_2$ layer is sandwiched by two Si-N bilayers. The optimized lattice constant is 2.88 Å which is consistent with the previous theoretical result [20]. The crystal symmetry of $VSi_2N_4$ is $D_{3h}$, and the inversion symmetry is broken like $2H$ TMDCs. We also find that $VSi_2N_4$ has a different formula and structure compared with MXene. The latter has specific formula $M_{n+1}X_nT_x$, where M (early transition metal) layers are interleaved by X (carbon/nitrogen) layers, and the surface is terminated by T (oxygen/hydroxyl/fluorine) [31,32]. Furthermore, we calculate the electron localization function [see Fig. 1(b)] to elucidate bonding types in $VSi_2N_4$. For the nearest-neighboring (NN) V and N atoms, electrons are mainly localized around N, which indicates an ionic bonding; highly localized electrons between the NN Si and N atoms suggest that there is covalent bonding between them. The phonon spectra [see Fig. 1(c)] demonstrate that $VSi_2N_4$ is dynamically stable.

Next, we focus on the magnetic properties of $VSi_2N_4$. According to Goodenough-Kanamori-Anderson rules [33–35], the superexchange coupling between two V atoms through an intervening N atom is FM since the bonding angle of V-N-V (90.26°) is very close to 90.00°. By comparing the energy difference of FM and antiferromagnetic (AFM) states of a $2 \times 1 \times 1$ supercell, we found that the NN exchange coupling $J$ between V atoms is FM with a magnitude of 29.70 meV. To determine the magnetic anisotropy energy (MAE) of $VSi_2N_4$, we calculate the energy difference between different spin directions of V atoms when SOC effect is considered. Here, we choose the energy when the magnetization orientation is parallel to the positive $x$ axis ($+x$) as a reference, and the corresponding coordinate is shown in Fig. 1(a). It can be seen in Fig. 1(d) that $VSi_2N_4$ has an easy magnetization plane; i.e., there is no energy consumption when magnetization rotates in the plane of the 2D layer. The coexistence of local magnetic moments (1.2 $\mu_B$ in V $3d$ orbitals) and easy magnetization plane indicates that $VSi_2N_4$ belongs to the family of 2D $XY$ magnets. For a 2D $XY$ magnet, the magnetic order can be stabilized under a finite size limit, and the Berezinsky-Kosterlitz-Thouless transition [36] could occur at a critical temperature ($T_c$) which can be estimated as $T_c = 0.89\, J/k_B$ [37,38], where the $k_B$ is the Boltzmann constant. With $J = 29.70$ meV, we obtain that the $T_c$ for $VSi_2N_4$ is around 307 K, which is above room temperature.

For obtaining the accurate electronic states, we test the influence of $U_{\text{eff}}$ on band structures of $VSi_2N_4$ monolayer as shown in Fig. S1 in the Supplemental Material [39]. One can see that the $VSi_2N_4$ is half-metallic when $U_{\text{eff}} = 0$ eV, and as $U_{\text{eff}}$ increases, $VSi_2N_4$ becomes an indirect band-gap semiconductor with valleys appearing at the $-K$ and $+K$ points. When $U_{\text{eff}}$ increases to 3 eV, $VSi_2N_4$ becomes a direct band-gap semiconductor (see $U_{\text{eff}} = 3$ eV of Fig. S1 [39]), and the valence band maximum (VBM) and conduction band minimum (CBM) consisting of electrons with the same spin just locate at the $-K$ and $+K$ points, which is very consistent with the band structure obtained from HSE06. These results indicate that $VSi_2N_4$ is a material with valley properties. In the following discussion, we choose $U_{\text{eff}} = 3$ eV to show in detail how spin and valley are coupled with each other. Since the magnetic anisotropy of $VSi_2N_4$ is IP, we calculate the band structure when SOC is included with the magnetization along $+x$, as shown in Fig. 2(a). One can see that the valley degeneracy is still preserved. By overcoming an energy barrier of 63.99 $\mu$eV, the magnetization orientation can be tuned from IP to OOP, and a relatively large valley polarization of 63.11 meV is induced [see Fig. 2(b)]. The valley polarization is quantitatively defined as the energy difference between VBM at $-K$ and $+K$, $\Delta E = E_{\text{VBM},+K} - E_{\text{VBM},-K}$. One can see that this valley polarization only appears at valence bands while it is degenerate at conduction bands. Notably, these results yield good comparison with the

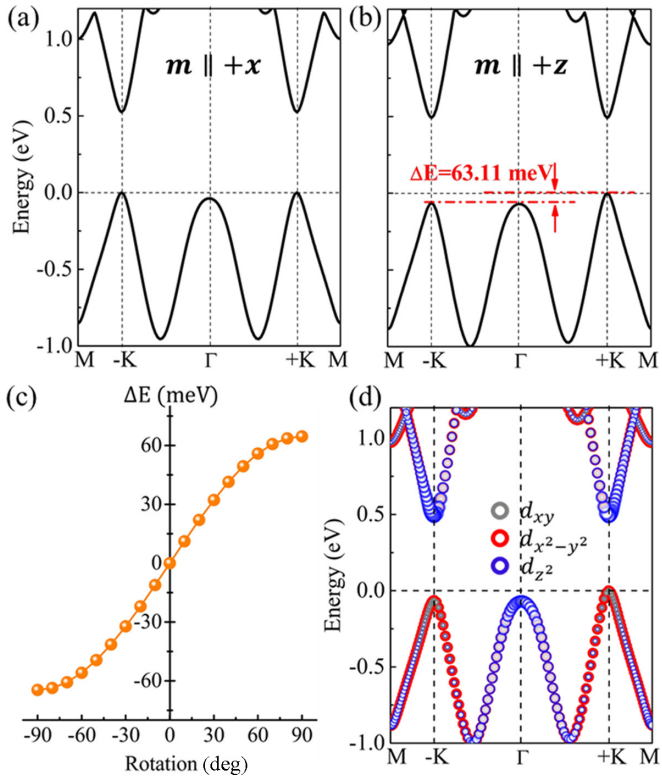


FIG. 2. The band structure of $VSi_2N_4$ monolayer with SOC when the magnetization is along (a) $+x$ and (b) $+z$. (c) The valley polarization $\Delta E$ as a function of magnetization orientation. The magnetization rotates from $-z$ to $+z$. (d) The orbital-resolved band structure of $VSi_2N_4$ monolayer with SOC when the magnetization is along $+z$.

band structures obtained from HSE06+SOC as illustrated in Fig. S2 [39], and an even larger polarization of 93.51 meV is achieved via HSE06+SOC calculations. In Fig. 2(c), we show the valley polarization as a function of magnetization orientation. The value of valley polarization varies from 63.11 to −63.11 meV continuously when the magnetization rotates from $+z$ to $-z$. Next, we derive the formula for describing the quantitative relationship between magnetization orientation and valley polarization. Since the VBM and CBM of $VSi_2N_4$ are both occupied by electrons with identical spin, we can ignore the interaction between spin-up and spin-down states. The SOC Hamiltonian can be written as [40,41]

$$\hat{H}_{\rm soc} \approx \hat{H}^0_{\rm soc} = \lambda \hat{S}_{z'}\left(\hat{L}_z \cos\theta + \tfrac{1}{2}\hat{L}_+ e^{-i\phi}\sin\theta + \tfrac{1}{2}\hat{L}_- e^{+i\phi}\sin\theta\right), \quad (1)$$

where $\hat{L}$ and $\hat{S}$ represent the orbital angular momentum and spin angular momentum, and $(x, y, z)$ and $(x', y', z')$ are the coordinate systems for $\hat{L}$ and $\hat{S}$, respectively. $\hat{L}_+ = \hat{L}_x + i\hat{L}_y$, and $\hat{L}_- = \hat{L}_x - i\hat{L}_y$. $\theta$ and $\phi$ are polar angles which define the spin orientation as shown in Fig. S3 in the Supplemental Material [39]. The VBM and CBM are dominated by $d_{xy}$, $d_{x^2-y^2}$, and $d_{z^2}$ orbitals of V atoms, respectively [see Fig. 2(d)]. The group symmetry of the $-K$ and $+K$ points is $C_{3h}$. Accordingly, the basis functions are chosen as $|\psi_c\rangle = |d_{z^2}\rangle$ and $|\psi_v^\tau\rangle = \sqrt{\frac{1}{2}}(|d_{x^2-y^2}\rangle + i\tau|d_{xy}\rangle)$, where $\tau = \pm 1$ represents the valley index. The energy levels for valleys at valence and conduction bands can be defined as $E_v^\tau = \langle\psi_v^\tau|\hat{H}^0_{\rm soc}|\psi_v^\tau\rangle$ and $E_c = \langle\psi_c|\hat{H}^0_{\rm soc}|\psi_c\rangle$, respectively. Consequently, the energy difference between valleys at the $-K$ and $+K$ points is given by

$$E_v^+ - E_v^- = i\langle d_{x^2-y^2}|\hat{H}^0_{\rm soc}|d_{xy}\rangle - i\langle d_{xy}|\hat{H}^0_{\rm soc}|d_{x^2-y^2}\rangle, \quad (2a)$$

$$E_c^+ - E_c^- = 0. \quad (2b)$$

Obviously, when the SOC effect is considered, the valley degeneracy at the valence bands is broken while it still stays degenerate for the conduction bands, which is consistent with the calculated band structure of $VSi_2N_4$. The basis functions $|d_{x^2-y^2}\rangle$ and $|d_{xy}\rangle$ have the form

$$|d_{x^2-y^2}\rangle = \frac{1}{\sqrt{2}}(|d_{+2}\rangle + |d_{-2}\rangle), \quad (3a)$$

$$|d_{xy}\rangle = \frac{1}{\sqrt{2}}[-i(|d_{+2}\rangle - |d_{-2}\rangle)], \quad (3b)$$

which results in $\hat{H}^0_{\rm soc}|d_{xy}\rangle \propto -2i\cos\theta|d_{x^2-y^2}\rangle + \frac{i\sin\theta}{\sqrt{2}}(e^{-i\phi}|d_{-1}\rangle - e^{+i\phi}|d_{+1}\rangle)$ and $\hat{H}^0_{\rm soc}|d_{x^2-y^2}\rangle \propto 2i\cos\theta|d_{xy}\rangle + \frac{\sin\theta}{\sqrt{2}}(e^{-i\phi}|d_{-1}\rangle + e^{+i\phi}|d_{+1}\rangle)$. Inserting this relationship into Eq. (2a), we obtain $E_v^+ - E_v^- \propto 4\cos\theta$ which means that the valley splitting will gradually disappear when spin rotates from OOP to IP. This result is consistent with the variation of valley splitting which is obtained from first-principles calculations [see Fig. 2(c)]. Notably, the similar behavior of valley polarization has also been reported in the $Mn/WS_2$ [17] and $Nb_3I_8$ monolayer [38].

In addition, we construct an effective Hamiltonian for $VSi_2N_4$ as the spin orientation along OOP:

$$H(k) = \boldsymbol{I}_s \otimes \left[v_f(\tau\sigma_x k_x + \sigma_y k_y) + \frac{\Delta}{2}\sigma_z\right] + \tau S_z(\lambda_u\sigma_+ + \lambda_l\sigma_-) - S_z(B_u\sigma_+ + B_l\sigma_-), \quad (4)$$

where the $v_f$ is the Fermi velocity, $\Delta$ is the gap, and $\lambda_u$ ($\lambda_l$) is the SOC parameter for the upper (lower) band. $B_u$ ($B_l$) is the effective exchange splitting for the upper (lower) band, which originates from the intrinsic ferromagnetism of V atoms. In this model, we choose the upper (lower) band instead of the valence (conduction) band [21]. The $S_\alpha$ and $\sigma_\alpha$ ($\alpha = x, y, z$) represent Pauli matrices for real spin and valley pseudospin, respectively. $\sigma_\pm$ is defined as $\frac{1}{2}(\sigma_0 \pm \sigma_z)$. As shown in Fig. S4 in the Supplemental Material [39], the band structures obtained from the model agrees with DFT results very well, with the fitting parameters in units of eV: $v_f = 2.15$, $\Delta = 0.64$, $\lambda_u = -0.0026$, $\lambda_l = 0.042$, $B_u = 1.49$, and $B_l = 0.73$. One can see that the value of effective exchange splitting $B_u$ ($B_l$) is large, reflecting the strong internal ferromagnetic field of $VSi_2N_4$ which splits the spin-down and spin-up states. The combination of intrinsic FM coupling and SOC effect of localized $3d$ electrons of V generates the valley polarization in $VSi_2N_4$ when the magnetization is OOP.

The valley polarization can give rise to AVHE in $VSi_2N_4$. To demonstrate this, we calculate the Berry curvature of $VSi_2N_4$ from Kubo formula derivation [42]:

$$\Omega(\boldsymbol{k}) = -\sum_n \sum_{n' \neq n} f_n 2\mathrm{Im}\frac{\langle\psi_{n\boldsymbol{k}}|v_x|\psi_{n'\boldsymbol{k}}\rangle\langle\psi_{n'\boldsymbol{k}}|v_y|\psi_{n\boldsymbol{k}}\rangle}{(E_{n'} - E_n)^2}, \quad (5)$$

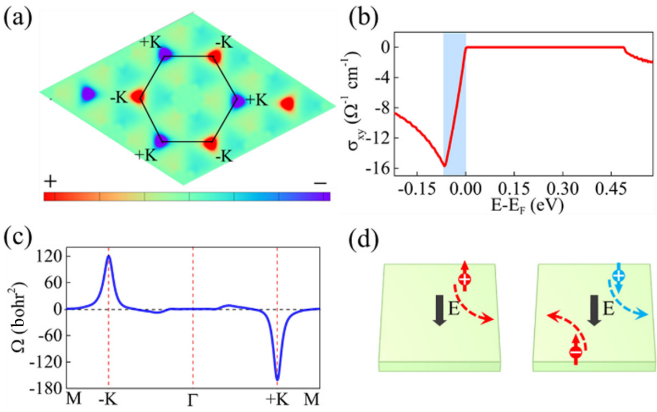


FIG. 3. For the $VSi_2N_4$ monolayer: the distributions of Berry curvature (a) in the whole Brillouin zone and (b) along the high-symmetry points. (c) The anomalous Hall conductivity as a function of $E_F$. (d) The schematics of the anomalous valley Hall effect under hole doping (left panel) and light irradiation (right panel). The magnetization is along $+z$. The electrons and holes in valley $+K$ are denoted by white $-$, $+$ in the dark circles, and the red and blue arrows represent spin-up and spin-down states.

where $f_n$ is the Fermi-Dirac distribution function, $v$ is the velocity operator, and $E_n$ is the eigenvalue of Bloch wave function $\psi_{nk}$. Figures 3(a) and 3(b) show the calculated Berry curvatures as a contour map in the whole 2D Brillouin zone and as a curve along the high-symmetry path. The Berry curvatures have opposite signs and different absolute values at the $-K$ and $+K$ points while it close to zero at other points in reciprocal space. Under an IP electrical field, the electrons or holes will acquire an anomalous velocity $v \sim \boldsymbol{E} \times \Omega(\boldsymbol{k})$. For $VSi_2N_4$, by shifting the Fermi level ($E_F$) between the $-K$ and $+K$ valleys in the valence bands, the spin-up holes from the $+K$ valley move to one side of the sample under an IP electrical field [see left panel in Fig. 3(d)], resulting in the net Hall current. Based on the formula [43]

$$\sigma_{xy} = \frac{e^2}{h}\frac{1}{2\pi}\int_{\mathrm{BZ}} d\boldsymbol{k}^2 \Omega(\boldsymbol{k}), \tag{6}$$

we calculated the anomalous Hall conductivity $\sigma_{xy}$. As shown in the shadow area of Fig. 3(c), the valley-polarized $\sigma_{xy}$ is achieved when the $E_F$ falls between the VBM of the $-K$ and $+K$ valleys, confirming the existence of AVHE. Moreover, by the excitation of linearly polarized light with frequency satisfying $\Delta_{+K}/\hbar \leqslant \omega \leqslant \Delta_{-K}/\hbar$, the spin-up electrons and spin-down holes from the $+K$ valley will be generated and accumulate on the opposite boundary of the sample under an IP electrical field as shown in the right panel of Fig. 3(d). Here, $\Delta_{+K}$ and $\Delta_{-K}$ represent the band gaps of the $+K$ and $-K$ valleys, respectively.

To obtain valley polarization in $VSi_2N_4$, the spin orientation is required to be OOP. However, the magnetic anisotropy of pristine $VSi_2N_4$ is IP. We already know that MAE is normally dominated by electronic states nearby the $E_F$ and the elements with relatively strong SOC [44,45]. Therefore, the $d_{xy}$, $d_{x^2-y^2}$, and $d_{z^2}$ orbitals of the V atoms possibly play crucial roles in determining the MAE of $VSi_2N_4$. Since $d_{xy}$ and $d_{x^2-y^2}$ are both IP orbitals, the MAE of $VSi_2N_4$ will be effectively tuned by biaxial strain as indicated by the blue line in Fig. 4(a). Notably, the magnetic anisotropy of $VSi_2N_4$ is tuned from IP to OOP when tensile strain reaches 4%. Moreover, as strain is in the range of 4%–8%, valley properties are still preserved as shown in Fig. S5 [39]. Due to the perpendicular magnetic anisotropy, the spontaneous valley polarization around 70 meV [see the orange line in Fig. 4(a)] has been generated in $VSi_2N_4$ under strain. Next, we choose the $VSi_2N_4$ under 6% strain as an example to exhibit valley-dependent transport properties. Figure S6 [39] shows the band structures when SOC effect is considered, and one can see that the valley polarization appears at CBM resulting from the occupation of $d_{xy}$ and $d_{x^2-y^2}$ states according to previous model analysis. Similar to the pristine $VSi_2N_4$, Berry curvatures have the opposite signs and different absolute values at the $-K$ and $+K$ points as shown in Figs. 4(b) and 4(c). When the $E_F$ is shifted between the $-K$ and $+K$ valleys in the conduction bands, spin-up electrons from the $-K$ valley will acquire the anomalous velocity [$v \sim \boldsymbol{E} \times \Omega(\boldsymbol{k})$ ] and accumulate at one boundary of the sample under an IP electrical field as

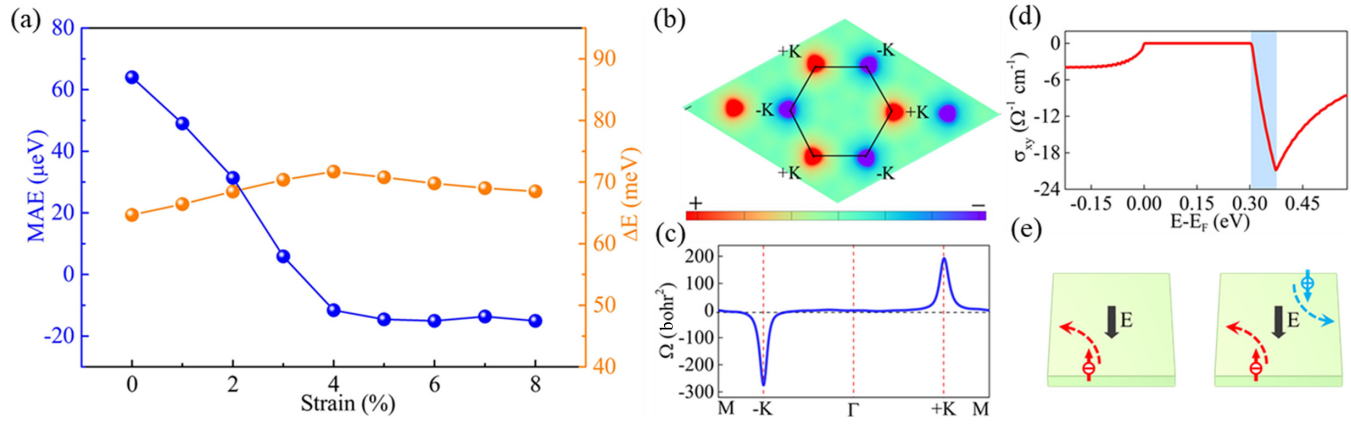


FIG. 4. (a) The magnetic anisotropy (blue line) and valley polarization (orange line) as functions of strain. For the $VSi_2N_4$ monolayer under 6% tensile strain: the distributions of Berry curvature (b) in the whole Brillouin zone and (c) along the high-symmetry points. (d) The anomalous Hall conductivity as a function of $E_F$. (e) The schematics of the anomalous valley Hall effect under electron doping (left panel) and light irradiation (right panel). The magnetization is along $+z$. The electrons and holes in valley $-K$ are denoted by dark $-$, $+$ in the hollow circles, and the red and blue arrows represent spin-up and spin-down states.

illustrated in the left panel of Fig. 4(e). Naturally, the valley-polarized $\sigma_{xy}$ is generated [see the shaded area of Fig. 4(d)], which demonstrates the existence of AVHE in $VSi_2N_4$ under strain. The spin-up electrons and spin-down holes from the $-K$ valley can also be excited by the linearly polarized light of the frequency satisfying $\Delta_{-K}/\hbar \leqslant \omega \leqslant \Delta_{+K}/\hbar$ and move to the opposite sides of the sample under an IP electrical field as shown in the right panel of Fig. 4(e).

## IV. CONCLUSION

In summary, via first-principles calculations, we find that the $VSi_2N_4$ monolayer is a ferromagnetic semiconductor with valley-contrasting physics. The intrinsic $VSi_2N_4$ is a *XY* magnet with a magnetic critical temperature over 300 K. By rotating the magnetization orientation from IP to OOP, the valley polarization of 63.11 meV can be achieved on the valence bands of $VSi_2N_4$, which results in the AVHE. Moreover, based on model analysis, we unveil that valley splitting is proportional to the cosine function of the polar angle $\theta$ of spin, and the combination of intrinsic FM exchange coupling and SOC of localized 3*d* electrons of V gives rise to the valley depolarization in $VSi_2N_4$ when spin is OOP. More interestingly, under 4% tensile strain, the magnetic anisotropy of $VSi_2N_4$ can be tuned from IP to OOP, and spontaneous valley polarization is generated, indicating that the AVHE can be realized in $VSi_2N_4$ without manipulating the magnetization orientation. Our work unveils the spin-valley coupling in $VSi_2N_4$, which makes $VSi_2N_4$ hopefully applicable in valleytronic and spintronic nanodevices.

## ACKNOWLEDGMENTS

This work was supported by the National Natural Science Foundation of China (Grant No. 11874059); Key Research Program of Frontier Sciences, CAS, Grant No. ZDBS-LY-7021; Beijing National Laboratory for Condensed Matter Physics; and Natural Science Foundation of Zhejiang Province (Grant No. LR19A040002) .

[1] D. Xiao, W. Yao, and Q. Niu, Valley-Contrasting Physics in Graphene: Magnetic Moment and Topological Transport, Phys. Rev. Lett. **99**, 236809 (2007).

[2] W. Yao, D. Xiao, and Q. Niu, Valley-dependent optoelectronics from inversion symmetry breaking, Phys. Rev. B **77**, 235406 (2008).

[3] D. Xiao, G. Liu, W. Feng, X. Xu, and W. Yao, Coupled Spin and Valley Physics in Monolayers of $MoS_2$ and Other Group-VI Dichalcogenides, Phys. Rev. Lett. **108**, 196802 (2012).

[4] T. Cao, G. Wang, W. Han, H. Ye, C. Zhu, J. Shi, Q. Niu, P. Tan, E. Wang, B. Liu, and J. Feng, Valley-selective circular dichroism of monolayer molybdenum disulphide, Nat. Commun. **3**, 887 (2012).

[5] X. Li, T. Cao, Q. Niu, J. Shi, and J. Feng, Coupling the valley degree of freedom to antiferromagnetic order, Proc. Natl. Acad. Sci. USA **110**, 3738 (2013).

[6] J. R. Schaibley, H. Yu, G. Clark, P. Rivera, J. S. Ross, K. L. Seyler, W. Yao, and X. Xu, Valleytronics in 2D materials, Nat. Rev. Mater. **1**, 1 (2016).

[7] K. F. Mak, K. L. McGill, J. Park, and P. L. McEuen, The valley Hall effect in $MoS_2$ transistors, Science **344**, 1489 (2014).

[8] J. Lee, K. F. Mak, and J. Shan, Electrical control of the valley Hall effect in bilayer $MoS_2$ transistors, Nat. Nanotechnol. **11**, 421 (2016).

[9] H. Zeng, J. Dai, W. Yao, D. Xiao, and X. Cui, Valley polarization in $MoS_2$ monolayers by optical pumping, Nat. Nanotechnol. **7**, 490 (2012).

[10] S. Liu, A. G. D. Águila, X. Liu, Y. Zhu, Y. Han, A. Chaturvedi, P. Gong, H. Yu, H. Zhang, W. Yao, and Q. Xiong, Room-temperature valley polarization in atomically thin semiconductors via chalcogenide alloying, ACS Nano **14**, 9873 (2020).

[11] G. Aivazian, Z. Gong, A. M. Jones, R. Chu, J. Yan, D. G. Mandrus, C. Zhang, D. Cobden, W. Yao, and X. Xu, Magnetic control of valley pseudospin in monolayer $WSe_2$, Nat. Phys. **11**, 148 (2015).

[12] A. Srivastava, M. Sidler, A. V. Allain, D. S. Lembke, A. Kis, and A. Imamoğlu, Valley Zeeman effect in elementary optical excitations of monolayer $WSe_2$, Nat. Phys. **11**, 141 (2015).

[13] Z. Ye, D. Sun, and T. F. Heinz, Optical manipulation of valley pseudospin, Nat. Phys. **13**, 26 (2017).

[14] D. MacNeill, C. Heikes, K. F. Mak, Z. Anderson, A. Kormanyos, V. Zolyomi, J. Park, and D. C. Ralph, Breaking of Valley Degeneracy by Magnetic Field in Monolayer $MoSe_2$, Phys. Rev. Lett. **114**, 037401 (2015).

[15] P. Back, M. Sidler, O. Cotlet, A. Srivastava, N. Takemura, M. Kroner, and A. Imamoğlu, Giant Paramagnetism-Induced Valley Polarization of Electrons in Charge-Tunable Monolayer $MoSe_2$, Phys. Rev. Lett. **118**, 237404 (2017).

[16] R. Peng, Y. Ma, S. Zhang, B. Huang, and Y. Dai, Valley polarization in Janus single-layer MoSSe via magnetic doping, J. Phys. Chem. Lett. **9**, 3612 (2018).

[17] J. Li, L. Gu, and R. Wu, Possible realization and protection of valley-polarized quantum Hall effect in $Mn/WS_2$, Phys. Rev. B **101**, 024412 (2020).

[18] C. Zhao, T. Norden, P. Zhang, P. Zhao, Y. Cheng, F. Sun, J. P. Parry, P. Taheri, J. Wang, Y. Yang, T. Scrace, K. Kang, S. Yang, G. Miao, R. Sabirianov, G. Kioseoglou, W. Huang, A. Petrou, and H. Zeng, Enhanced valley splitting in monolayer $WSe_2$ due to magnetic exchange field, Nat. Nanotechnol. **17**, 757 (2017).

[19] T. Norden, C. Zhao, P. Zhang, R. Sabirianov, A. Petrou, and H. Zeng, Giant valley splitting in monolayer $WS_2$ by magnetic proximity effect, Nat. Commun. **10**, 4163 (2019).

[20] Y. Hong, Z. Liu, L. Wang, T. Zhou, W. Ma, C. Xu, S. Feng, L. Chen, M. Chen, D. Sun, X. Chen, H. Cheng, and W. Ren, Chemical vapor deposition of layered two-dimensional $MoSi_2N_4$ materials, Science **369**, 670 (2020).

[21] W. Tong, S. Gong, X. Wan, and C. Duan, Concepts of ferrovalley material and anomalous valley Hall effect, Nat. Commun. **7**, 13612 (2016).

[22] G. Kresse and J. Hafner, *Ab initio* molecular dynamics for liquid metals, Phys. Rev. B **47**, 558 (1993).

[23] G. Kresse and J. Furthmuller, Efficient iterative schemes for *ab initio* total-energy calculations using a plane-wave basis set, Phys. Rev. B **54**, 11169 (1996).

[24] G. Kresse and J. Furthmuller, Efficiency of *ab-initio* total energy calculations for metals and semiconductors using a plane-wave basis set, Comput. Mater. Sci. **6**, 15 (1996).

[25] Y. Wang and J. P. Perdew, Correlation hole of the spin-polarized electron gas, with exact small-wave-vector and high-density scaling, Phys. Rev. B **44**, 13298 (1991).

[26] G. Kresse and D. Joubert, From ultrasoft pseudopotentials to the projector augmented-wave method, Phys. Rev. B **59**, 1758 (1999).

[27] H. L. Zhuang and R. G. Hennig, Stability and magnetism of strongly correlated single-layer $VS_2$, Phys. Rev. B **93**, 054429 (2016).

[28] A. V. Krukau, O. A. Vydrov, A. F. Izmaylov, and G. E. Scuseria, Influence of the exchange screening parameter on the performance of screened hybrid functionals, J. Chem. Phys. **125**, 224106 (2006).

[29] A. Togo and I. Tanaka, First principles phonon calculations in materials science, Scr. Mater. **108**, 1 (2015).

[30] N. Marzari, A. A. Mostofi, J. R. Yates, I. Souza, and D. Vanderbilt, Maximally localized Wannier functions: Theory and applications, Rev. Mod. Phys. **84**, 1419 (2012).

[31] Y. Gogotsi and B. Anasori, The rise of MXenes, ACS Nano **13**, 8491 (2019).

[32] B. Anasori, M. R. Lukatskaya, and Y. Gogotsi, 2D metal carbides and nitrides (MXenes) for energy storage, Nat. Rev. Mater. **2**, 16098 (2017).

[33] B. Goodenough, Theory of the role of covalence in the Perovskite-type manganites [La, *M*(II)] $MnO_3$, Phys. Rev. **100**, 564 (1955).

[34] J. Kanamori, Superexchange interaction and symmetry properties of electron orbitals, J. Phys. Chem. Solids **10**, 87 (1959).

[35] P. W. Anderson, New approach to the theory of superexchange interactions, Phys. Rev. **115**, 2 (1959).

[36] J. M. Kosterlitz and D. J. Thouless, Ordering, metastability and phase transitions in two-dimensional systems, J. Phys. C: Solid State Phys. **6**, 1181 (1973).

[37] J. F. Fernàndez, M. F. Ferreira, and J. Stankiewicz, Critical behavior of the two-dimensional *XY* model: A Monte Carlo simulation, Phys. Rev. B **34**, 292 (1986).

[38] M. Ashton, D. Gluhovic, S. B. Sinnott, J. Guo, D. A. Stewart, and R. G. Hennig, Two-dimensional intrinsic half-metals with large spin gaps, Nano Lett. **17**, 5251 (2017).

[39] See Supplemental Material at http://link.aps.org/supplemental/10.1103/PhysRevB.103.085421 for band structures of $VSi_2N_4$ obtained from (1) GGA+$U$ and HSE06 without considering SOC effects, and (2) HSE06+SOC; (3) the coordinate systems are used for describing orbital and spin angular momentum; (4) comparison between the band structures calculated from DFT results and low-energy effective model; (5) band structures of $VSi_2N_4$ under the 4%–8% tensile strains when SOC is included; and (6) orbital-resolved band structures of $VSi_2N_4$ under 6% tensile strain.

[40] D. Dai, H. J. Xiang, and M.-H. Whangbo, Effects of spin-orbit coupling on magnetic properties of discrete and extended magnetic systems, J. Comput. Chem. **29**, 2187 (2008).

[41] R. Peng, Y. Ma, X. Xu, Z. He, B. Huang, and Y. Dai, Intrinsic anomalous valley Hall effect in single-layer $Nb_3I_8$, Phys. Rev. B **102**, 035412 (2020).

[42] D. J. Thouless, M. Kohmoto, M. P. Nightingale, and M. den Nijs, Quantized hall Conductance in a Two-Dimensional Periodic Potential, Phys. Rev. Lett. **49**, 405 (1982).

[43] N. Nagaosa, J. Sinova, S. Onoda, A. H. MacDonald, and N. P. Ong, Anomalous Hall effect, Rev. Mod. Phys. **82**, 1539 (2010).

[44] Q. Cui, J. Liang, B. Yang, Z. Wang, P. Li, P. Cui, and H. Yang, Giant enhancement of perpendicular magnetic anisotropy and induced quantum anomalous Hall effect in graphene /$NiI_2$ heterostructures via tuning the van der Waals interlayer distance, Phys. Rev. B **101**, 214439 (2020).

[45] Q. Cui, J. Liang, Z. Shao, P. Cui, and H. Yang, Strain-tunable ferromagnetism and chiral spin textures in two-dimensional Janus chromium dichalcogenides, Phys. Rev. B **102**, 094425 (2020).